Geochemical and petrological characterization of gem opals from Wegel Tena, Wollo, Ethiopia: opal formation in an Oligocene soil

Benjamin Rondeau[1,*], Bénédicte Cenki-Tok[2,3], Emmanuel Fritsch[4], Francesco Mazzero[5], Jean-Pierre Gauthier[6], Yves Bodeur[1], Eyassu Bekele[7], Eloïse Gaillou[8] & Dereje Ayalew[9]

[1]*University of Nantes, Laboratoire de Planétologie et Géodynamique, UMR-CNRS 6112, 2 rue de la Houssinière BP 92208, F-44322 Nantes Cedex 3, France*

[2]*Institute for Geology, University of Bern, Baltzerstr. 1+3, CH-3012 Bern, Switzerland*

[3]*Now at: Géosciences, University of Montpellier 2, UMR5243, 34095 Montpellier Cedex 5, France*

[4]*University of Nantes, Institut des Matériaux Jean Rouxel, UMR-CNRS 6205, 2 rue de la Houssinière BP 32229, F-44322 Nantes Cedex 3, France*

[5]*Opalinda, 59 rue Sainte-Anne, 75002 Paris, France*

[6]*Centre de Recherches Gemmologiques, 2 rue de la Houssinière, BP 92208, 44322 Nantes cedex 3, France*

[7]*Eyaopal, Addis Ababa, Ethiopia*

[8]*Department of Mineral Sciences, Smithsonian Institution, Washington, DC 20560, USA*

[9]*Department of Earth Sciences, Addis Ababa University, Ethiopia*

**Corresponding author (e-mail: benjamin.rondeau@univ-nantes.fr)*

ABSTRACT: Gem opals from Wegel Tena, Wollo Province, Ethiopia, occur in Oligocene rhyolitic ignimbrites. They display a unique geochemistry, with some samples yielding the highest Ba concentrations ever recorded. They are generally much richer in chemical impurities than opals from other localities. For example, the sum Al+Fe or the sum Na+Mg+Ca+K+Ba are often higher. These geochemical features make them easy to distinguish from other opals worldwide. We observed strong geochemical variations and some good positive correlations in our samples, such as Al+Fe vs. Na+Mg+Ca+K+Ba, Al vs Ca, or Ba vs Ca. This shows that the crystallography of opal has controlled, at least in part, the incorporation of chemical impurities, although opal is not well-crystallized. In addition, the multimodal distributions of several chemical impurities (e.g. U vs Sr, Al vs Ca, Ba vs Ca, etc.) suggest at least two origins of silica: weathering of feldspars and weathering of volcanic glass. In addition, opals from Wegel Tena contain numerous well-preserved microscopic plant fossils. Moreover, their host rock exhibits features typical of pedogenesis (abundant clays, desiccation cracks, and grain size sorting). We propose that the opals at Wegel Tena formed during the Oligocene period when volcanic emissions stopped for a time long enough to allow weathering of ingimbrites and therefore liberation of silica. This accompanied the formation of soil and development of plant life, and some plants were trapped in opal.

SUPPLEMENTARY MATERIAL: The totality of the chemical analyses is available at http://www.geolsoc.org.uk/SUP18519.

KEYWORDS: *opal formation, Ethiopia, pedogenesis, plant fossils, chemical impurities*

A new deposit of play-of-colour opal was discovered in 2008 in the Wollo province of Ethiopia (Mazzero *et al.* 2009; Rondeau *et al.* 2009; Rondeau *et al.* 2010*a*). The percentage of gem quality material is surprisingly high in this deposit. Many samples are of outstanding beauty and value, and this material is very resistant to breaking unlike most opals in the market today (Rondeau *et al.* 2010*a*). Hence, this opal deposit has a potential of becoming a major commercial source of opal in the near future.

The deposit occurs in an Oligocene volcano-sedimentary sequence of alternating basalt and rhyolitic ignimbrite layers. The opal deposit forms a single, thin layer (*c.* 1 m thick) within and concordant with an ignimbrite layer in the volcanic sequence. The deposit extends laterally for several hundreds of metres. Like most opals found in volcanic environments, such as in Mexico, Kazakhstan or in the Shewa province of Ethiopia (Gaillou *et al.* 2008*a*), the opals studied are opal-CT (cristobalite-tridymite) (Rondeau *et al.* 2010*a*, *b*).

In this work, we describe the textural and microscopic features of opals from Wegel Tena, and the petrography of their host rock. We investigate in detail their chemical compositions, focusing on chemical differences between samples and

DOI: 10.1144/1467-7873/10-MINDEP-058

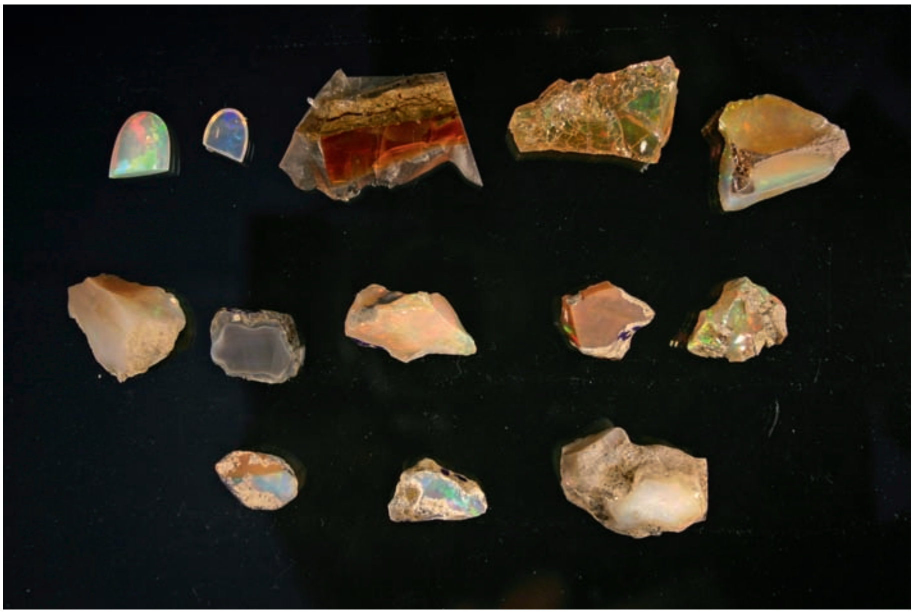

Fig. 1. Photograph of the 13 samples of Wegel Tena opals studied for geochemistry. From left to right, top row: samples 1073, 1076, 1078, 1103, 1111; middle row: samples 5, 6, 7, 8, 9; bottom row: samples 10, 11, 12. Photo by B. Rondeau.

zoning within individual opal specimens in order to assess their geological conditions of formation. Understanding these conditions of formation may help in developing guidelines for opal exploration in this area. Indeed, its mode of formation appears to differ somewhat from the few models proposed so far for the formation of gem opal deposits. In addition, geochemical characteristics are commonly used in gemology as an indicator of gem's geographical provenance (e.g. Abduriyim *et al.* 2006; Peucat *et al.* 2007; Rossman 2009). The samples studied in this article have been acquired in the gem market but were initially collected from the Wegel Tena area. We could not collect them in the field for security reasons (i.e. only the miners are authorized to access the opal-bearing area).

MATERIALS AND METHODS

Chemical analyses on 13 samples were performed with LA-ICP-MS. Some of the samples were previously investigated by Rondeau *et al.* (2010*a*, *b*). They represent the range of colour and transparency (from colourless to dark brown, and from transparent to opaque) and play-of-colour of opals in the Wegel Tena deposit (Fig. 1). Samples 7, 11, 12, 1073, and 1076 are white translucent with play-of-colour. Samples 8 and 1078 are dark brown with strong play-of-colour; in addition, sample 8 shows columnar structures that we called digit patterns (Rondeau *et al.* 2010*a*). Sample 1103 is orange transparent with play-of-colour. Sample 6 has a black, nearly opaque body colour with little play-of-colour. The other samples are zoned. Samples 9 and 10 exhibit two distinct zones: one white translucent and the other orange transparent, both with play-of-colour. One zone in sample 1111 is orange-yellow and translucent with no play-of-colour, the other zone is white translucent with play-of-colour. In samples 10 and 1111, the contact between the two zones is sharp (even under the microscope), whereas it is blurry in sample 9. Sample 5 shows a light brown core without play-of-colour and a white, translucent rim with slight play-of-colour.

The samples of opal were prepared as thin sections and polished for the electron microprobe and LA-ICP-MS analyses. LA-ICP-MS element composition data were obtained at the Institute for Geological Sciences in Bern. The system consists of a pulsed 193 nm ArF Excimer laser (Lambda Physik, Germany) with an energy-homogenized (Microlas, Germany) beam profile coupled with an ELAN DRCe quadrupole mass spectrometer (QMS; Perkin Elmer, Canada). Laser parameters were set to 16 J/cm^2 energy density with a 15 ns pulse duration and 10 Hz repetition rate. Pit sizes used were 60 and 90 μm. Laser-ablation aerosol was carried to the ICP-QMS by a mixed He-H_2-Ar carrier gas. Nebulizer, auxiliary, and cool gas flows were set to 0.80, 0.70, and 16.0 l/min Ar, respectively. RF power was 1500 kV. The analytical set-up was tuned for optimum performance across the entire mass range. Daily optimization of the analytical conditions was done to satisfy a ThO production rate below 0.2% (i.e. Th/ThO intensity ratio is <0.002) and to achieve robust plasma conditions monitored by a Th/U sensitivity ratio of 1 as determined using a SRM610 glass standard. Further details on the setup and optimization strategies are given in Pettke (2008). Analyses were performed in sequence, and each ablation was stored individually as a transient (i.e. time resolved) signal acquired in peak-hopping mode. Data acquisition parameters were one sweep per reading, with 200–300 readings per replicate. Dwell time per isotope was 10 ms. The certified glass standard SRM 610 was used as an external standard to calibrate analyte sensitivities, and bracketing standardization provided a linear drift correction. Data reduction was performed with the program SILLS (Guillong *et al.* 2008). LA-ICP-MS measurements have been internally normalized to their true SiO_2 (range: 83–95 wt%). These were determined on each individual domains and samples with a JEOL JXA 8200 electron probe at the University of Bern, operating at 15 kV accelerating voltage and 15 nA beam current, using orthoclase as an external standard.

In order to examine its typical host rock and its relationship to the opal, we acquired a chemical map of the most abundant elements (Si, Al, K, Na) across a rock/opal boundary. We used a JEOL 5800 LV Scanning Electron Microscope (SEM) at the Institut des Matériaux Jean Rouxel, University of Nantes. This SEM is equipped with a PGT (Princeton Gamma Tech) energy dispersion (EDS) IMIX-PTS detector. The SEM was operated at a beam accelerating potential of 20 kV, a 0.3 nA current, with a 37° take-off angle of the detector. Additional samples were studied under the microscope for their inclusions.

RESULTS & DISCUSSION

Texture and microscopic features

Plant fossils

Numerous samples of opal show inclusions, which are consistent with fossil plants such as stems, twigs, and roots (Figs 2, 3). These are replaced by silica in the form of opal, but still they often contain some carbon. The disposition of the plant fossils inside the opal indicates that the opal formed when the plants were still living organisms, or just after their death. They appear 'frozen' in a silica matrix.

Pedogenic features

The opals are associated with ignimbrite weathered into abundant clays. Fig. 4 shows a sample of opal in contact with its weathered (and argillized) ignimbrite host rock. Several platelets and lenses of clay are embedded in the opal. A chemical map of an opal in contact with its host rock shows that the main phenocrysts in the ignimbrite are represented by alkali feldspars, which are weathered to various degrees (Fig. 5). Some quartz and very few plagioclase phenocrysts are observed. There is a graduation of the mineral grain size in the rhyolitic ignimbrite host-rock, with decreasing grain size of feldspar phenocrysts as opal abundance increases. Observations of weathered ignimbrite under the microscope reveal numerous cracks and contraction features in clays, which are filled-in with opal, suggesting desiccation of clays after swelling. These features are typical of pedogenesis, which resulted in the development of soil at the surface of the ignimbrite. These observations strongly indicate that the opals were associated with the pedogenesis of the rhyolitic ignimbrite host rock.

Fig. 2. Plant fossil in opal sample #1100 (picture width is 4 mm, diameter of the stem is *c.* 1 mm). Photo by B. Rondeau.

Fig. 3. Plant fossil in opal sample #1332 (picture width is 3 cm, diameter of stems is *c.* 1 mm). Photo by F. Mazzero.

Fig. 4. Typical irregular contact of opal with its host-rock (weathered ignimbrite of rhyolitic composition). Sample #1124, *c.* 10 × 6 × 3 cm. Photo by B. Rondeau.

Element geochemistry of the Wegel Tena opals

All results of chemical analysis are given in the Supplementary Material. We observed multiple differences in the properties (chemistry, colour, transparency, play-of-colour vs common opal) and sometimes zoning in the individual samples, which deliver information on the petrogenetic formation of opal. The presence and concentration of chemical impurities in opals reflects primarily the host-rock composition, as silica in opal comes from its alteration (as shown in Gaillou *et al.* 2008*b*). In addition, some of the differences in properties might arise from fractionation during opal precipitation, as proposed by Brown *et al.* (2004) and Thomas *et al.* (2006). However, the incorporation of chemical impurities in the opal silica network must respect the electroneutrality of the mineral; that is, although opal is poorly crystallized, its network is dominated by Si-O bonds in the three dimensions.

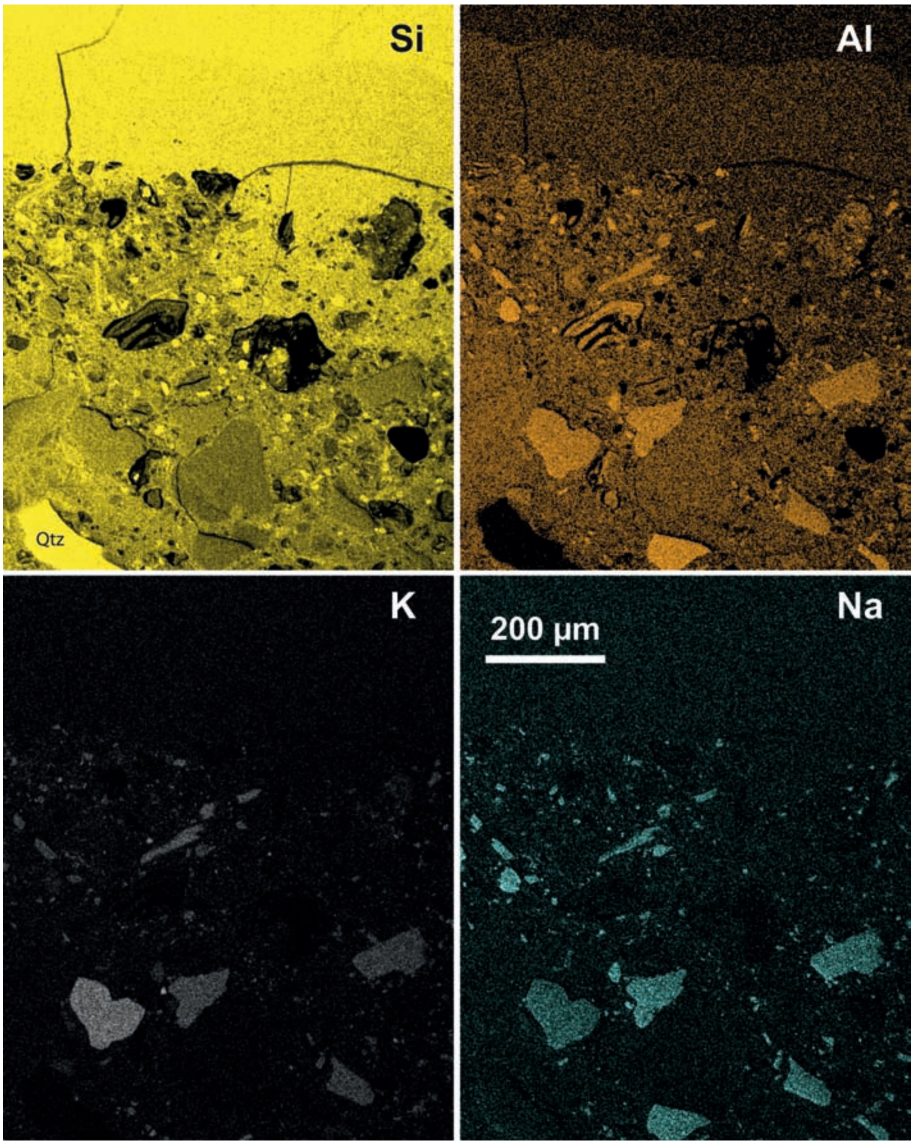

Fig. 5. Chemical maps obtained by SEM analysis for Si, Al, K and Na in a single matrix sample. The horizontal band at the top is opal, the bottom part is the weathered ignimbrite. Note that some feldspars remain unweathered while others are strongly weathered. One remaining quartz crystal is present at the bottom left corner (Qtz). Grain sizes in the ignimbrite decrease toward opal.

Chemical impurities and optical properties

The concentration of chemical impurities is highly variable between and within the studied samples. Aluminum, the most abundant impurity in the studied opals, varies from 2 700 ppm (which is few for opal) to 4% (which is a lot) (cf. Gaillou *et al.* 2008*b*). Calcium is also abundant (480 ppm to 1%). Potassium ranges from 1 600–11 000 ppm. Iron is highly variable (from 2–13 500 ppm) with a tendency to be higher in coloured samples. The higher Fe values in the orange samples are not surprising because Fe is the colouring agent of fire opal (Fritsch *et al.* 2002; Gaillou *et al.* 2008*b*). Sodium ranges from 430–2 000 ppm. Magnesium ranges from 54 to 1 500 ppm. Manganese is generally low (<100 ppm), except in the orange domain of sample 10 and in sample 6. Strontium is generally low (from 4–162 ppm), although white and brownish samples typically contain 100–160 ppm Sr. Zirconium ranges from 13 to 584 ppm. Barium ranges from 6–756 ppm. The darkest samples (vivid orange and chocolate brown) are depleted in Ba (<100 ppm). Translucent brownish samples and white samples have generally high Ba contents (up to 756 ppm), suggesting that Ba might form precipitates (such as $BaSO_4$) that scatter light. Sample 12 is an exception; it is a white creamy sample and shows the lowest Ba content (<10 ppm). Sample 6, which is homogeneously black, shows the lowest concentrations of Al, Ca, K, Na, and Mg, but the highest of Mn. Hence, the black colour is likely due to the presence of some black Mn oxides.

Geochemical variations within zoned samples

Samples 1111 and 10 are remarkably zoned. This zonation affects the chemical concentrations of some elements, but surprisingly, not all. In particular, Fe, Ti, Mn, Nd, V, Y, Nb, Pb, Th, and U are significantly higher in the orange part of these samples than in the white part (see Fig. 6 and Supplementary Material). In contrast, Na, K, Ba, As, Rb, Sr, Zr, Mo, and Cd show no variation with the zonation. The other elements show no systematic variation. A similar behaviour has previously been observed by Brown *et al.* (2004) and Thomas *et al.* (2006)

Fig. 6. Results of LA-ICP-MS analyses of geochemical concentrations in samples of Wegel Tena opals. Concentrations of SiO_2 is expressed in wt%, whereas those of other elements are expressed in µg/g. The darker the grey background in this figure, the darker the orange body-colour of the opal sample. For each sample, the first line (in italic) gives the average composition and the second line (in bold) the range of composition. See detailed analyses in the Supplementary Material

sample	analysis Nr.	Li	B	Na	Mg	Al	SiO2	K	Ca	Sc
6-average		*0.53*	*0.27*	*446*	*60*	*2885*	*95.0*	*1764*	*830*	*2.15*
6-range-	**n=10**	**0,28-0,72**	**0,18-0,29**	**429-462**	**54-71**	**2702-3189**	**95.0**	**1665-1867**	**745-1083**	**1,81-2,31**
10-orange-average		*5.56*	*2.84*	*1110*	*1436*	*32888*	*86.6*	*8652*	*9680*	*2.77*
10-orange-range	**n=6**	**3,17-9,98**	**1,94-4,99**	**1079-1139**	**1305-1593**	**28959-40087**	**86.0**	**8155-9056**	**9535-10004**	**2,40-3,43**
10-white-average		*< 0.15*	*1.03*	*1159.28*	*978.62*	*24394*	*86.6*	*9409.07*	*8855.67*	*1.56*
10-white-range	**n=6**	**< 0.15**	**<0,43-1,20**	**1125-1187**	**960-980**	**24057-24699**	**86.6**	**8247-9917**	**8498-8960**	**1,45-1,68**
FT1076-average		*0.09*	*1.57*	*1939*	*1048*	*25422*	*87.8*	*11146*	*9014*	*1.47*
FT1076-range	**n=10**	**<0,08-0,11**	**1,32-2,19**	**1923-1971**	**1017-1065**	**24590-26776**	**87.8**	**10960-11303**	**8783-9258**	**1,35-1,69**
FT1073-average		*0.13*	*0.43*	*1203*	*913*	*19540*	*83.4*	*8203*	*7230*	*1.44*
FT1073-range	**n=7**	**<0,11-0,16**	**<0,31-0,54**	**1188-1223**	**891-945**	**19428-20272**	**83.4**	**8106-8353**	**7144-7353**	**1,39-1,57**
FT1103-average		*1.13*	*0.31*	*1661*	*41*	*5362*	*92.8*	*4925*	*1421*	*2.46*
FT1103-range	**n=9**	**0,40-1,49**	**<0,21-0,31**	**838-2074**	**5-187**	**3150-10203**	**92.8**	**3642-5813**	**496-4475**	**1,72-2,87**
FT1078-average		*6.2*	*0.21*	*1472*	*114*	*7180*	*92.2*	*4875*	*1423*	*1.57*
FT1078-range	**n=12**	**4,8-7,4**	**<0,13-0,23**	**827-1810**	**98-125**	**5795-11600**	**92.2**	**4273-6036**	**938-4905**	**1,49-1,66**
FT1111-dark-average		*0.76*	*0.64*	*876*	*842*	*19131*	*91.0*	*8013*	*7262*	*1.33*
FT1111-dark-range	**n=8**	**0,49-1,15**	**0,49-0,85**	**837-936**	**795-873**	**17690-20233**	**91.0**	**7140-8667**	**6889-7522**	**1,11-1,48**
FT1111-white-average		*0.15*	*0.68*	*932*	*794*	*18688*	*91.0*	*8424*	*7050*	*1.42*
FT1111-white-range	**n=7**	**<0,09-0,18**	**<0,37-0,79**	**873-1072**	**775-812**	**17760-19854**	**91.0**	**8184-8702**	**6691-7627**	**1,30-1,51**
5-average		*0.65*	*1.25*	*1460*	*840*	*22857*	*84.8*	*9823*	*8570*	*1.25*
5-range	**n=16**	**0,17-1,80**	**0,75-2,32**	**1410-1508**	**797-927**	**20414-24326**	**84.8**	**8900-10082**	**7946-9217**	**1,11-1,47**
8-average		*1.72*	*1.04*	*1735*	*737*	*25082*	*86.1*	*9840*	*9572*	*1.36*
8-range	**n=6**	**1,46-1,95**	**0,77-1,53**	**1712-1783**	**730-750**	**24834-25309**	**86.1**	**9072-10150**	**9432-10097**	**1,31-1,42**
7-average		*0.18*	*2.54*	*1165*	*936*	*21302*	*85.2*	*8629*	*8000*	*1.25*
7-range	**n=5**	**<0,12-0,22**	**0,75-9,16**	**1121-1224**	**904-989**	**20632-22148**	**85.2**	**7883-8927**	**7613-8570**	**1,20-1,34**
12-average		*<0,17*	*0.33*	*638*	*56*	*4346*	*93.4*	*1865*	*1107*	*1.24*
12-range	**n=5**	**<0,17**	**0,19-0,47**	**30713**	**2,0-84**	**3916-4959**	**93.4**	**1740-2228**	**950-1303**	**1,18-1,35**
9-average		*0.20*	*0.77*	*1253*	*543*	*17568*	*83.6*	*7577*	*6649*	*1.30*
9-range	**n=8**	**<0,09-0,27**	**<0,38-1,02**	**1174-1307**	**527-560**	**16801-19000**	**83.6**	**7115-7985**	**6129-6987**	**1,04-1,43**
11-average		*0.29*	*0.88*	*1191*	*759*	*17889*	*84.1*	*7864*	*6686*	*1.31*
11-range	**n=8**	**<0,09-0,46**	**<0,36-1,35**	**1149-1249**	**731-797**	**17164-18463**	**84.1**	**7407-8217**	**6229-7067**	**1,27-1,38**

Ti	V	Mn	Fe	Co	Ni	Cu	Zn	As	Rb	Sr	Y
53	*0.10*	*265*	*74*	*0.02*	*0.84*	*0.08*	*0.40*	*0.18*	*8.3*	*9.7*	*0.39*
42-124	**0,08-0,15**	**119-364**	**58-133**	**<0,02**	**0,55-1,16**	**<0,06-0,14**	**0,28-0,75**	**0,10-0,23**	**7,93-9,27**	**9,0-11,6**	**0,31-0,89**
734	*2.79*	*161*	*4579*	*1.11*	*1.89*	*1.22*	*16*	*0.25*	*76*	*161*	*9.0*
451-1497	**1,65-5,61**	**121-258**	**3155-7970**	**0,87-1,50**	**1,12-2,98**	**0,91-1,92**	**13-21**	**0,12-0,56**	**58-88**	**154-166**	**7,4-11,6**
1.41	*0.04*	*1.50*	*2.32*	*0.01*	*<0,44*	*0.31*	*0.36*	*0.08*	*87*	*157*	*4.33*
40575	**<0,03-0,06**	**0,81-3,61**	**<1,43-2,15**	**< 0.02**	**<0,44**	**0,16-0,39**	**<0,23-0,56**	**<0,11**	**61-95**	**154-158**	**3,52-4,53**
11.7	*0.17*	*3.00*	*42*	*0.04*	*<0,06*	*0.54*	*5.3*	*<0,06*	*73*	*157*	*0.16*
10,1-15,2	**0,13-0,22**	**2,88-3,19**	**32-47**	**0,03-0,06**	**<0.60**	**0,34-0,91**	**1,2-11,6**	**<0,06**	**71-74**	**152-162**	**0,13-0,19**
1.86	*0.03*	*0.66*	*4.59*	*<0,02*	*<0,10*	*0.18*	*0.34*	*<0,08*	*67*	*137*	*0.63*
1,60-2,24	**<0,02-0,03**	**0,53-0,88**	**3,71-5,71**	**<0,02**	**<0,10**	**0,08-0,23**	**<0,23-0,38**	**<0,08**	**65-68**	**131-140**	**0,59-0,65**
23	*0.05*	*14*	*90*	*<0,01*	*1.60*	*0.17*	*0.45*	*0.33*	*24*	*17*	*0.08*
9,0-37	**<0,03-0,07**	**10,0-26**	**43-284**	**<0,01**	**0,76-2,31**	**<0,05-0,35**	**0,23-0,69**	**<0,05-0,38**	**17-30**	**7,0-50**	**0,04-0,14**
631	*1.42*	*78*	*823*	*0.06*	*0.28*	*0.23*	*8.9*	*0.08*	*23*	*22*	*4.4*
564-679	**1,31-1,59**	**71-82**	**740-933**	**0,04-0,09**	**<0,24-0,38**	**0,14-0,29**	**7,8-10,3**	**<0,06-0,11**	**19-28**	**16-61**	**3,9-4,9**
192	*0.34*	*5.5*	*184*	*0.05*	*0.49*	*0.20*	*0.90*	*<0,07*	*49*	*117*	*1.06*
192-244	**0,15-0,86**	**3,4-81**	**95-314**	**0,03-0,10**	**<0,37-0,49**	**0,14-0,28**	**0,76-1,35**	**<0,08**	**40-54**	**110-124**	**0,87-1,19**
4.5	*0.06*	*2.9*	*103*	*0.02*	*<0,50*	*0.24*	*0.53*	*<0,10*	*51*	*117*	*0.72*
2,2-10,0	**<0,02-0,16**	**1,8-4,6**	**13-303**	**<0,01-0,03**	**<0,50**	**0,19-0,27**	**0,24-0,80**	**<0,10**	**45-54**	**110-133**	**0,64-0,80**
147	*0.49*	*13*	*245*	*0.03*	*0.32*	*0.53*	*1.57*	*0.08*	*63*	*144*	*0.63*
30-310	**0,26-0,90**	**3,0-36**	**60-594**	**<0,01-0,04**	**<0,47**	**0,20-1,17**	**<0,21-4,02**	**<0,06-0,09**	**45-66**	**132-154**	**0,18-1,63**
715	*1.26*	*35*	*869*	*0.04*	*0.27*	*0.46*	*4.53*	*0.08*	*64*	*141*	*3.44*
673-761	**1,18-1,31**	**30-38**	**599-957**	**0,03-0,05**	**0,23-<0,41**	**0,36-0,53**	**3,88-4,85**	**<0,05-0,11**	**57-66**	**138-149**	**3,30-3,55**
81	*0.08*	*2.0*	*40*	*0.01*	*0.71*	*0.22*	*0.46*	*<0,07*	*69*	*145*	*0.74*
29-165	**0,03-0,15**	**1,3-3,0**	**26-63**	**<0,02**	**<0,29-0,71**	**0,16-0,24**	**0,32-0,64**	**<0,07**	**60-73**	**138-154**	**0,65-0,85**
2.81	*0.04*	*5.1*	*32*	*<0,01*	*0.25*	*<0,08*	*0.23*	*0.08*	*10.3*	*5.7*	*0.18*
2,08-3,26	**<0,02-0,05**	**4,0-8,1**	**4,0-65**	**<0,01**	**<0,60**	**<0,08**	**<0,31**	**<0,05-<0,10**	**9,5-11,9**	**4,9-6,4**	**0,17-0,19**
4.6	*0.04*	*2.6*	*84*	*0.01*	*<1,24*	*0.29*	*0.23*	*<0,13*	*53*	*97*	*0.25*
2,8-7,5	**<0,02-0,05**	**2,0-3,4**	**23-165**	**<0,03**	**<1,24**	**0,10-0,67**	**<0,44**	**<0,13**	**45-55**	**91-103**	**0,20-0,29**
15	*0.05*	*1.55*	*54*	*0.01*	*0.56*	*0.30*	*0.32*	*<0,10*	*72*	*113*	*2.22*
10,0-20	**<0,03-0,07**	**1,17-2,15**	**9,0-137**	**<0,02**	**<0,67**	**0,18-0,61**	**<0,27-0,40**	**<0,10**	**65-75**	**107-119**	**1,88-2,42**

Zr	Nb	Mo	Cd	Ba	La	Ce	Pr	Nd	Sm	Eu	Gd
26	*2.68*	*0.02*	*0.21*	*75*	*0.27*	*0.81*	*0.08*	*0.35*	*0.08*	*0.02*	*0.08*
25-31	**2,22-5,84**	**<0,04**	**0,14-0,32**	**45-100**	**0,21-0,57**	**0,57-1,83**	**0,06-0,20**	**0,22-0,87**	**0,05-0,19**	**0,01-0,04**	**0,03-0,11**
423	*21*	*0.17*	*0.12*	*718*	*11.0*	*16.6*	*1.91*	*7.4*	*1.40*	*0.32*	*1.41*
332-584	**13-45**	**0,09-0,39**	**0,08-0,15**	**651-756**	**8,4-16,7**	**10,3-32,0**	**1,54-2,69**	**6,0-9,9**	**1,14-1,90**	**0,26-0,42**	**1,17-1,87**
267	*0.41*	*<0,07*	*0.12*	*730.56*	*2.52*	*0.21*	*0.34*	*1.57*	*0.24*	*0.06*	*0.36*
201-317	**0,37-0,46**	**<0,07**	**<0,14**	**679-752**	**2,17-2,67**	**0,20-0,22**	**0,30-0,36**	**1,44-1,75**	**0,19-0,28**	**0,06-0,07**	**0,30-0,39**
158	*0.94*	*<0,06*	*0.12*	*264*	*0.22*	*0.27*	*0.02*	*0.10*	*0.04*	*0.010*	*0.03*
127-191	**0,77-1,06**	**<0,06**	**<0,16**	**263-270**	**0,12-0,45**	**0,21-0,40**	**0,01-0,03**	**0,08-0,12**	**<0,05**	**<0,010**	**<0,04**
66	*0.25*	*<0,03*	*<0,11*	*340*	*0.49*	*0.22*	*0.05*	*0.21*	*0.04*	*0.01*	*0.07*
61-79	**0,22-0,30**	**<0,03**	**<0,11**	**326-348**	**0,39-0,80**	**0,20-0,27**	**0,04-0,06**	**0,14-0,27**	**<0,03**	**<0,01**	**0,05-0,10**
73	*1.10*	*<0,03*	*0.16*	*35*	*0.07*	*0.20*	*0.02*	*0.06*	*0.03*	*0.009*	*0.022*
34-206	**0,60-1,61**	**<0,03**	**<0,09-0,15**	**17-64**	**0,03-0,10**	**0,09-0,30**	**<0,01-0,04**	**0,04-0,11**	**<0,02-0,03**	**<0,005-0,014**	**<0,048**
113	*23.9*	*0.07*	*0.11*	*61*	*6.9*	*16.1*	*1.72*	*6.7*	*1.40*	*0.31*	*1.20*
104-147	**21,9-26,7**	**<0,04-0,09**	**<0,06-0,13**	**53-72**	**6,0-7,5**	**14,6-17,5**	**1,50-1,87**	**6,1-7,2**	**1,16-1,56**	**0,26-0,34**	**1,00-1,42**
152	*6.44*	*0.03*	*0.12*	*232*	*0.32*	*0.54*	*0.06*	*0.26*	*0.06*	*0.02*	*0.09*
100-234	**3,5-8,17**	**<0,05**	**<0,14**	**219-251**	**0,23-0,55**	**0,29-1,17**	**0,05-0,13**	**0,14-0,46**	**0,04-0,16**	**<0,01-0,03**	**0,07-0,14**
120	*0.32*	*<0,07*	*0.17*	*237*	*0.13*	*0.18*	*0.02*	*0.10*	*0.04*	*0.01*	*0.05*
72-237	**0,26-0,44**	**<0,07**	**<0,08-0,17**	**223-264**	**0,10-0,22**	**0,09-0,42**	**0,01-0,05**	**0,07-0,12**	**<0,05**	**<0,02**	**0,04-0,07**
174	*6.4*	*0.03*	*0.09*	*217*	*0.61*	*1.47*	*0.17*	*0.65*	*0.16*	*0.05*	*0.12*
92-366	**1,5-13,2**	**<0,02-0,04**	**<0,14**	**206-225**	**0,10-1,73**	**0,21-4,18**	**0,02-0,49**	**0,08-1,82**	**0,05-0,48**	**<0,01-0,14**	**0,03-0,34**
156	*27*	*0.08*	*0.11*	*271*	*2.37*	*5.78*	*0.69*	*2.89*	*0.68*	*0.19*	*0.65*
122-244	**26-29**	**0,07-0,09**	**<0,08-0,14**	**263-280**	**2,19-2,46**	**5,15-6,24**	**0,63-0,73**	**2,61-3,07**	**0,62-0,72**	**0,17-0,20**	**0,59-0,77**
110	*3.85*	*<0,04*	*0.15*	*292*	*0.53*	*0.72*	*0.09*	*0.38*	*0.07*	*0.02*	*0.07*
63-200	**1,51-7,68**	**<0,04**	**<0,10-0,22**	**283-304**	**0,45-0,63**	**0,54-1,14**	**0,07-0,12**	**0,30-0,50**	**0,03-0,09**	**0,02-0,03**	**0,05-0,10**
14.3	*0.69*	*<0,07*	*<0,18*	*7.6*	*0.05*	*0.06*	*0.01*	*0.04*	*<0,04*	*<0,010*	*<0,03*
12,9-18,9	**0,64-0,73**	**<0,07**	**<0,18**	**6,3-10,1**	**0,02-0,08**	**0,02-0,09**	**<0,01**	**<0,03-0,06**	**<0,04**	**<0,010**	**<0,03**
109	*0.45*	*<0,09*	*0.10*	*181*	*0.05*	*0.08*	*0.01*	*0.05*	*<0,06*	*<0,02*	*0.04*
78-203	**0,35-0,60**	**<0,09**	**<0,26**	**167-186**	**0,04-0,06**	**0,05-0,13**	**<0,02**	**<0,03-0,07**	**<0,06**	**<0,02**	**<0,02-0,04**
81	*0.67*	*0.03*	*0.12*	*295*	*1.48*	*0.48*	*0.23*	*0.94*	*0.17*	*0.03*	*0.20*
51-126	**0,54-0,87**	**<0,04**	**<0,19**	**275-304**	**1,25-1,63**	**0,40-0,56**	**0,20-0,25**	**0,82-1,08**	**0,14-0,19**	**0,02-0,05**	**0,15-0,30**

Tb	Dy	Ho	Er	Tm	Yb	Lu	Pb	Th	U
0.010	*0.08*	*0.01*	*0.03*	*0.007*	*0.03*	*0.006*	*0.08*	*0.08*	*1.22*
0,008-0,020	**0,05-0,16**	**0,01-0,03**	**<0,02-0,08**	**<0,015-0,021**	**0,01-0,04**	**<0,010**	**0,04-0,13**	**0,05-0,15**	**0,95-1,56**
0.20	*1.34*	*0.28*	*0.79*	*0.12*	*0.75*	*0.11*	*0.59*	*2.75*	*0.43*
0,17-0,28	**1,04-2,10**	**0,22-0,41**	**0,56-1,06**	**0,09-0,19**	**0,50-1,29**	**0,08-0,19**	**0,35-1,16**	**1,66-5,64**	**0,30-0,82**
0.05	*0.31*	*0.08*	*0.24*	*0.03*	*0.16*	*0.03*	*0.02*	*0.007*	*0.04*
0,05-0,05	**0,26-0,33**	**0,07-0,08**	**0,18-0,30**	**0,02-0,03**	**0,10-0,20**	**0,02-0,04**	**<0,03**	**<0,010**	**0,03-0,04**
0.004	*0.03*	*0.004*	*0.02*	*0.004*	*0.015*	*0.004*	*0.07*	*0.03*	*0.07*
<0,005	**0,01-0,04**	**<0,002-0,006**	**<0,01-0,03**	**<0,006**	**<0,03**	**<0,005**	**<0,03-0,18**	**0,02-0,03**	**0,06-0,08**
0.009	*0.05*	*0.014*	*0.05*	*0.01*	*0.04*	*0.006*	*0.02*	*0.008*	*0.04*
0,005-0,012	**<0,02-0,06**	**0,009-0,016**	**0,03-0,08**	**<0,01-0,04**	**<0,02-0,06**	**<0,010**	**<0,03**	**<0,011**	**0,03-0,04**
0.005	*0.019*	*0.004*	*0.018*	*0.004*	*0.024*	*0.005*	*0.07*	*0.05*	*0.77*
<0,004-0,007	**<0,013-0,026**	**<0,006**	**<0,021**	**<0,002-0,004**	**<0,037**	**<0,002-0,005**	**0,03-0,12**	**0,03-0,06**	**0,17-1,13**
0.17	*1.02*	*0.19*	*0.50*	*0.06*	*0.41*	*0.05*	*1.36*	*2.44*	*1.32*
0,14-0,19	**0,89-1,19**	**0,17-0,20**	**0,43-0,57**	**0,06-0,08**	**0,31-0,45**	**0,04-0,06**	**1,23-1,56**	**2,15-2,69**	**1,03-1,50**
0.014	*0.12*	*0.03*	*0.08*	*0.01*	*0.10*	*0.02*	*0.13*	*0.05*	*0.21*
0,007-0,024	**0,08-0,17**	**0,02-0,04**	**0,07-0,11**	**0,01-0,02**	**0,07-0,14**	**0,01-0,03**	**0,09-0,23**	**0,04-0,10**	**0,13-0,34**
0.007	*0.06*	*0.013*	*0.05*	*0.009*	*0.05*	*0.008*	*<0,03*	*0.008*	*0.03*
<0,004-0,010	**0,04-0,10**	**0,007-0,017**	**0,02-0,09**	**<0,010-0,011**	**0,02-0,10**	**<0,010**	**<0,03**	**<0,007-0,015**	**0,03-0,05**
0.02	*0.12*	*0.03*	*0.07*	*0.01*	*0.07*	*0.01*	*0.18*	*0.13*	*0.25*
<0,01-0,06	**0,03-0,32**	**<0,01-0,07**	**0,02-0,17**	**<0,01-0,03**	**<0,02-0,16**	**<0,01-0,02**	**<0,02-0,37**	**0,03-0,18**	**0,09-0,45**
0.10	*0.69*	*0.14*	*0.41*	*0.06*	*0.37*	*0.05*	*0.65*	*0.94*	*1.05*
0,09-0,11	**0,62-0,73**	**0,13-0,15**	**0,39-0,46**	**0,05-0,06**	**0,32-0,46**	**0,05-0,06**	**0,62-0,70**	**0,84-1,26**	**0,92-1,17**
0.012	*0.07*	*0.02*	*0.05*	*0.008*	*0.05*	*0.009*	*0.05*	*0.07*	*0.16*
0,010-0,013	**0,04-0,09**	**0,01-0,012**	**0,04-0,05**	**0,006-0,011**	**0,03-0,08**	**0,007-0,010**	**0,03-0,09**	**0,05-0,10**	**0,09-0,25**
0.004	*0.02*	*0.003*	*0.02*	*0.004*	*0.04*	*0.008*	*<0,03*	*0.017*	*0.22*
<0,015-0,005	**<0,01-0,02**	**<0,005**	**<0,01-0,03**	**<0,007**	**<0,02-0,06**	**0,006-0,009**	**<0,03**	**0,014-0,023**	**0,21-0,23**
0.003	*0.03*	*0.006*	*0.02*	*0.007*	*<0,05*	*0.006*	*0.06*	*0.014*	*0.06*
<0,005	**<0,02-0,04**	**<0,004-0,010**	**<0,03**	**<0,008**	**<0,05**	**<0,003-0,006**	**<0,02-0,06**	**0,010-0,021**	**0,05-0,07**
0.03	*0.22*	*0.05*	*0.15*	*0.020*	*0.12*	*0.02*	*0.02*	*0.018*	*0.05*
0,02-0,04	**0,19-0,27**	**0,03-0,05**	**0,12-0,18**	**0,013-0,024**	**0,10-0,15**	**0,01-0,03**	**<0,01-0,03**	**0,011-0,021**	**0,04-0,06**

in banded opals, and has been attributed by these authors to fractionation phenomenon.

Rare-earth element geochemistry

The REE abundances, which are normalized to the CI chondrite abundances given by McDonough & Sun (1995), are shown in Fig. 7. They range between 0.01 and 100, which is the classical range for opal (Gaillou *et al.* 2008*b*). Most samples show a nearly flat pattern with a more or less pronounced enrichment in LREE compared to HREE (Fig. 7a). In general, no anomalies are observed. Within a single sample, we usually observe a very homogeneous composition (e.g. in samples 7, 8, 11, 1073, 1076, and 1078). However, some samples show noticeable variation in composition (e.g. samples 5 and 1111-orange). Some samples (Fig. 7c) show a nearly flat pattern with very low REE concentrations and variable composition.

Rarely, a negative Ce anomaly is observed (e.g. samples 10-white and 11; Fig. 7b). Gaillou *et al.* (2008*b*) proposed that such Ce anomaly is likely due to the transformation of Ce^{3+} into Ce^{4+} under oxidizing conditions. However, the Ce anomaly was not present in the opal host rock, indicating that it developed during weathering. Interestingly, a very weak or absent Eu anomaly is observed in the host rock. This may be explained by the lack of plagioclase in the mother-rock.

Source of silica

Several sources of silica for the formation of opal have been proposed in the literature, and two are considered relevant here: (1) weathering of alkali feldspar into clays is a mineralogical reaction that frees silica; and (2) ignimbritic ashes of rhyolitic composition consist of minute silica-rich particles rich in glass, and water percolation in such ashes easily dissolves silica due to the very large contact surface. These two phenomena may operate together, or one can dominate locally, reflecting the local petrological heterogeneity (i.e. some micro-domains are rich in ashes, some others are richer in feldspar). The 'competition' between these two sources of silica may explain in part the geochemical variations observed in our set of samples.

Source of Ba

The Wollo opals exhibit considerable variations in Ba, from almost the lowest (6 ppm) to the highest ever recorded for an opal (756 ppm). Alkali feldspars are known to incorporate Ba in various amounts under the form of celsian or hyalophane (Gay & Roy 1968). Strongly localized variations in the degree of weathering of feldspars into clays in our samples may explain why Ba reached such high concentrations in some of the samples but is present in low concentrations in others. In addition, the variations in Ba concentration may be explained by the competition between the two considered possible sources of silica (i.e. feldspar weathering and ash leaching). Gaillou *et al.* (2008*b*) explained the distinction between sedimentary (strong alteration, high Ba contents of >110 ppm) and volcanic (less alteration, low Ba contents of <110 ppm) environments based on the degree of weathering of alkali feldspars. However, this criteria does not apply here because of the competition of different processes of silica production.

Geochemical correlations

We checked for possible relations between elements. Fig. 8 shows that Al and Ca are correlated in most of the studied samples (except in the orange domains of sample 10 with Al contents >30 000 ppm). The Al-Ca correlation becomes less

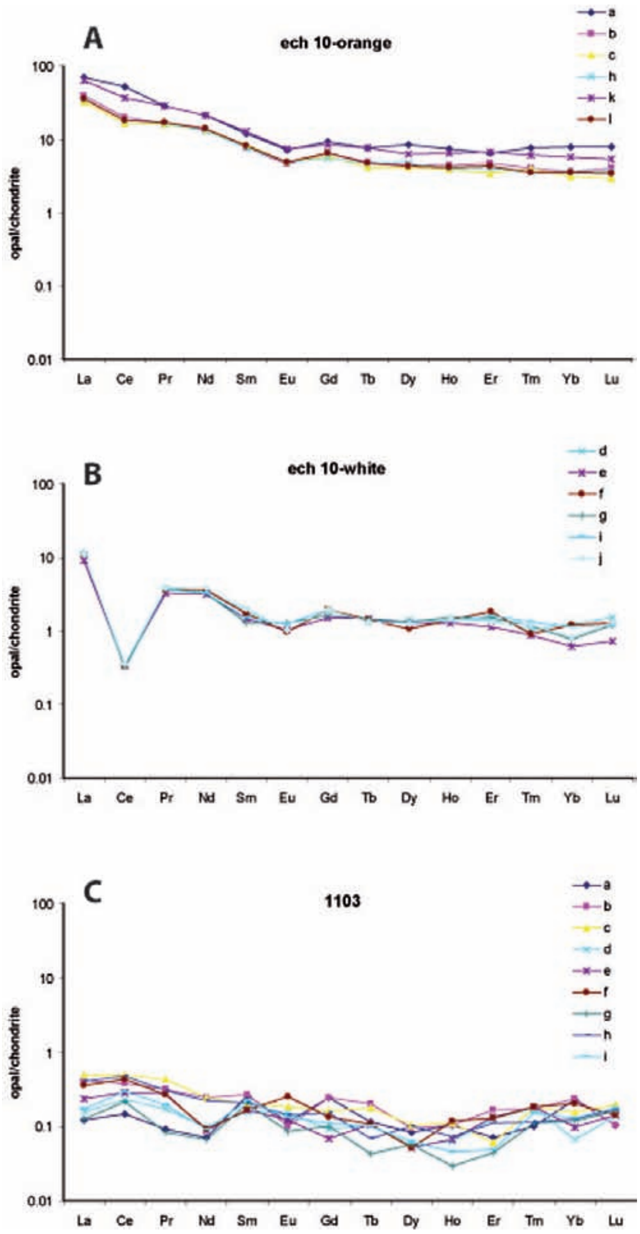

Fig. 7. Patterns of REEs in the studied opals from Wegel Tena. Lower case letters identifying each graph refer to the points of analysis per sample given in Fig. 6 and the Supplementary Material.

obvious as concentrations increase. Similarly, Ba and Ca (Fig. 9) roughly correlate in the studied samples (except in both domains of sample 10, with Ba >650 ppm). A similar correlation can be observed for Ca vs Sr, Ba vs Rb, and Ba vs Sr, although less clear than the Ba-Ca correlation.

Fig. 10 shows that the sum of trivalent ions (Al^{3+}, Fe^{3+}) correlates well with the sum of the main divalent and monovalent ions (Na^{+}, Ca^{2+}, K^{+}, Ba^{2+}, Mg^{2+}) in the Wegel Tena opals. This shows that the incorporation of cations in opal follows the rules of electroneutrality. As detailed in Gaillou *et al.* (2008*b*), the replacement of Si^{4+} by Al^{3+} or Fe^{3+} in the silica network induces a charge imbalance, which must be compensated by the contribution of divalent or monovalent cations, at a ratio of 1 monovalent ion to 1 trivalence, and 1 divalent ion to 2 trivalence. However, we observe that the highest values of Al+Fe (>30 000 ppm) do not follow this general trend. They

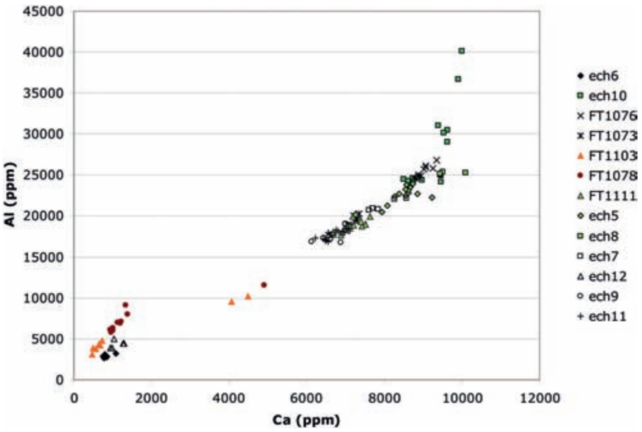

Fig. 8. Plots of concentrations of Al vs Ca in the Wegel Tena opals.

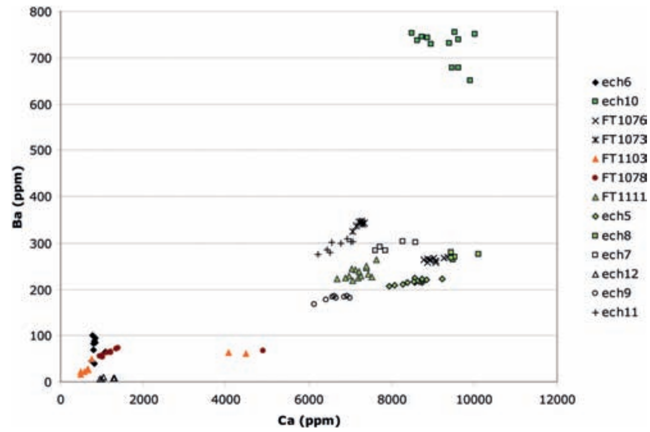

Fig. 9. Plots of concentrations of Ba vs Ca in the Wegel Tena opals.

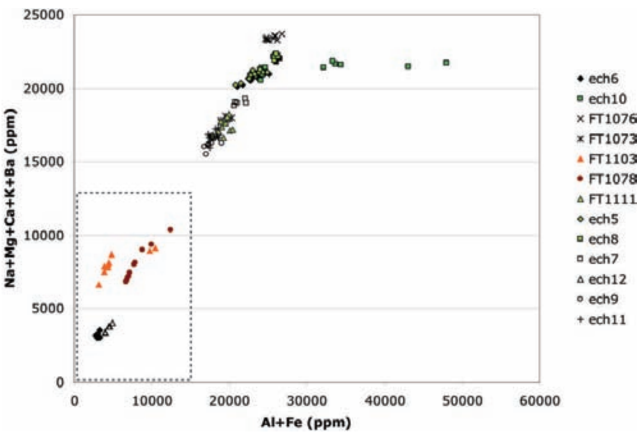

Fig. 10. Plots of the sum of concentrations of the main trivalent impurities (Al + Fe) vs. the sum of concentrations of the main mono- and trivalent impurities (Na+Mg+Ca+K+Ba) in opals from Wegel Tena. The dotted rectangle represents the field of values given in Gaillou *et al.* (2008*b*) for other opals worldwide.

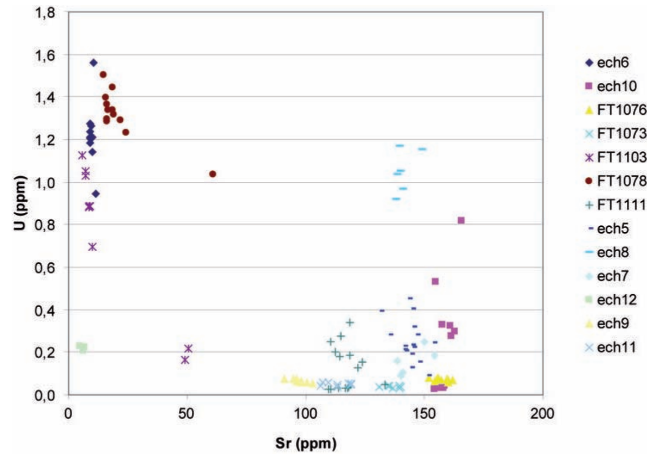

Fig. 11. Plots of concentrations of Sr vsU in the Wegel Tena opals.

correspond to sample 10-orange, which is either enriched in Al+Fe or depleted in Na+Ca+Mg+Ba+K.

Figs 8, 9, and 10 show, in addition to the general positive correlations, that the plots are distributed in at least two main ranges. Such a bimodal or multimodal distribution is observed occasionally for many other pairs of elements, with different trends for each range. This is the case of Si vs. Al, K or Ca. Figure 11 shows that samples depleted in U are generally rich in variable amounts of Sr, and vice-versa. This strongly supports the hypothesis of at least two sources of silica gel for the precipitation of opals. One source may be dominated by the weathering of feldspars (rich in K, Ba, Sr), because feldspars are enriched in Sr compared to volcanic glasses (Ren 2004). The other source may be dominated by the weathering of volcanic glass, because U is concentrated in volcanic glasses rather than in feldspars (Gray *et al.* 2011). Because the studied opals do not show homogeneous composition, we propose that the silica-bearing fluids did not experience intense circulation that would have homogenized the different sources.

Mode of formation

Fossilized plants along with carbonaceous matter in opal have been documented in several other deposits, such as in Virgin Valley in Nevada, USA (Zielinski 1982), silicified bones in Australia (Pewkliang *et al.* 2008) or silicified wood from Slovakia (Papp *et al.* 1998) and other localities. In such deposits, opal fills-in voids of wood cells or makes up wood cast. These silicification phenomena are diagenetic processes that occur after sediment burial. In contrast, plant fossils in our samples are embedded in opal, suggesting that opal formed in a silica-rich water where plants developed; hence, in a soil at the surface of the parent rock (i.e. rhyolitic ignimbrite).

The presence of abundant clays clearly demonstrates that the studied opals formed during an episode of weathering of the host ignimbrite. Chemical impurities (Al, Ca, and K in particular) are much more abundant in opals from Wegel Tena than in any other opal (cf. Gaillou *et al.* 2008*b*). In addition, we observed very strong variation in the concentration of many elements, even at the millimetre scale. These last two observations suggest that the silica-rich water did not circulate enough to homogenize the composition, nor to purify it from impurities. We suggest that during the Oligocene volcanic episode, the emission of volcanic ashes stopped for a time long enough to allow weathering of the ignimbrite, resulting in the formation of soil that supported plant life. Meteoric waters weathered the ignimbrite, liberating silica through the transformation of feldspars into clays, and through the weathering of volcanic glass particles.

This mode of formation is remarkably different from particular models proposed so far for the formation of gem, play-of-colour opal. One model states that fire opal from Mexico formed during late volcanic stages at relatively high temperature (Koivula *et al.* 1983). Another model proposes that water circulation in fractures and faults controlled the formation of opal in Slovakian andesites (Rondeau *et al.* 2004). In contrast, some Australian sedimentary opals formed during tectonic events (Pecover 2007) possibly combined to some weathering (Jones & Segnit 1966; Barnes & Townsend 1982). However, pink common opals from Peru and Mexico developed in quiet lake environments (Fritsch *et al.* 2004), and common opal can form in such environment (Rayot 1994).

Comparison with other deposits

It is essential to understand geological processes that control the geochemical signatures of opals in order to use the geochemical fingerprinting efficiently for the provenance determination. Most of the studied opals from Wegel Tena (i.e. about the two thirds of our sample set) contain much more impurities than opals from anywhere else (Fig. 10, dotted rectangle after Gaillou *et al.* 2008*b*) (cf. McOrist *et al.* 1994; McOrist & Smallwood 1995, 1997; Brown *et al.* 2004; Thomas *et al.* 2006; Pewkliang *et al.* 2008). For example, the sum Al+Fe or the sum Na+Mg+Ca+K+Ba is higher in many of the studied opals compared to other opals elsewhere. The high concentrations of chemical impurities in opals from Wegel Tena make them easy to differentiate from opals from all other deposits, and hence can be used efficiently as a provenance fingerprint. However, this criterion cannot be used on a small number of opals from Wegel Tena that contain low impurities content.

CONCLUSION

Opals from Wegel Tena, some of which yielded the highest Ba concentrations ever recorded, show a unique geochemistry. They generally contain much higher chemical impurities than other opals worldwide. They have geochemical fingerprints that clearly distinguish them from all opals mined in other areas worldwide. However, they also exhibit strong geochemical variations. Some positive correlations in geochemical compositions (such as Al+Fe vs Na+Mg+Ca+K+Ba, Al vs Ca, or Ba vs Ca) indicate that some of the chemical impurities were controlled by the crystallochemistry of opal. That is, although the Wegel Tena opals are poorly crystallized, they consist mostly of tri-dimensional networks of Si-O bonds. Concentrations of many elements in the studied opals follow various trends. This indicates that the fluid responsible for the mineralization was heterogeneous, and suggests that at least two sources of silica were involved in opal formation: weathering of feldspars into clays and weathering of volcanic glass. Microscopic observations reveal the presence of many plant fossils in the studied opals. In addition, the opals exhibit features that are characteristic of pedogenesis, such as abundant clays, desiccation features and grain size sorting. We propose that opals at Wegel Tena formed during a pause in the emission of ignimbrite ashes, when a soil could develop at the surface and support plant life. Further avenues of research of the genesis of the Wegel Tena opals include linking the observed chemical variations with spatial distribution, petrographic variations and variations of the degree of weathering. Such comparison and field observations may strongly strengthen the model proposed here.

BCT thanks T. Pettke for assistance during LA-ICP-MS analyses. The electron microprobe at the University of Bern is partly funded by the Swiss National Fond (Grant 200021-103479/1). SEM maps were acquired thanks to the help of Nicolas Stéphant and Stéphane Grolleau, IMN. We thank Thomas Cenki for collecting the samples studied here. We thank Antoine Bezos for constructive discussions on the interpretation of chemical analyses. This article has been considerably strengthened and clarified, thanks to Alan Pring, Lee Groat and John Carranza who reviewed it.

REFERENCES

Abduriyim, A., Kitawaki, H., Furuya, M. & Schwarz, D. 2006. "Paraíba"-type copper-bearing tourmaline from Brazil, Nigeria and Mozambique: chemical fingerprinting by LA-ICP-MS. *Gems & Gemology*, **42**, **1**, 4–21.

Barnes, L.C. & Towsend, I.J. 1982. *Opal - South Australia's gemstone*. Handbook no. 5, Department of Mines and Energy, Geological Survey of South Australia.

Brown, L.D., Ray, A.S. & Thomas, P.S. 2004. Elemental analysis of Australian amorphous banded opals by laser ablation ICP–MS. *Neues Jahrbuch für Mineralogie Monatshefte*, **9**, 411–424.

Fritsch, E., Ostroumov, M. et al. 2002. Mexican gem opals: nano- and micro-structure, origin of colour, comparison with other common opals of gemmological significance. *Australian Gemmologist*, **21**, 230–233.

Fritsch, E., Gaillou, E., Ostroumov, M., Rondeau, B. & Barreau, A. 2004. Relationship between nanostructure and optical absorption in fibrous pink opals from Mexico and Peru. *European Journal of Mineralogy*, **16**, 743–752.

Gaillou, E., Fritsch, E., Aguilar-Reyes, B., Rondeau, B., Post, J., Barreau, A. & Ostroumov, M. 2008*a*. Common gem opal: an investigation of micro- to nano-structure. *American Mineralogist*, **93**, 1865–1873.

Gaillou, E., Delaunay, A., Rondeau, B., Bouhnik-le Coz, M., Fritsch, E., Cornen, G. & Monnier, C. 2008*b*. The geochemistry of opals as evidence of their origin. *Ore Geology Reviews*, **34**, 113–126.

Gay, P. & Roy, N.N. 1968. The mineralogy of the potassium-barium feldspar series III: Subsolidus relationships. *The Mineralogical Magazine*, **36**, 914–932.

Gray, T.R., Hanley, J.J., Dostal, J. & Guillong, M. 2011. Magmatic enrichment of uranium, thorium, and Rare Earth Elements in late Paleozoic rhyolites of Southern New Brunswick, Canada: evidence from silicate melt inclusion. *Economic Geology*, **106**, 127–143.

Guillong, M., Meier, D.L., Allan, M.M., Heinrich, C.A. & Yardley, B.W.D. 2008. Appendix A6: Sills: A Matlab-based program for the reduction of laser ablation ICP-MS data of homogeneous materials and inclusions. *In*: Sylvester P. (ed.) *Laser Ablation ICP-MS in the Earth Sciences: Current Practices and Outstanding Issues*. Mineralogical Association of Canada, Vancouver, B.C.: Short Course Series, **40**, 328–333.

Jones, J.B. & Segnit, E.R. 1966. The occurrence and formation of opal at Coober Pedy and Andamooka. *Australian Journal of Sciences*, **29**, 129–133.

Koivula, J.I., Fryer, C.W. & Keller, P.C. 1983. Opal from Querétaro: occurrence and inclusions. *Gems and Gemology*, **19**, 87–98.

Mazzero, F., Gauthier, J.-P., Rondeau, B., Fritsch, E. & Bekele, E. 2009. Nouveau gisement d'opales d'Ethiopie dans la Province du Welo: Premières informations [New deposit of Ethiopian opals in the Wollo Province: Early information]. *Revue de Gemmologie a.f.g.*, **167**, 4–5 [in French].

McDonough, W.F. & Sun, S.-S. 1995. The composition of the Earth. *Chemical Geology*, **120**, 223–253.

McOrist, G.D., Smallwood, A. & Fardy, J.J. 1994. Trace elements in Australian opals using neutron activation analysis. *Journal of Radioanalytical and Nuclear Chemistry*, **185**, 293–303.

McOrist, G.D. & Smallwood, A. 1995. Trace elements in coloured opals using neutron activation analysis. *Journal of Radioanalytical and Nuclear Chemistry*, **198**, 499–510.

McOrist, G.D. & Smallwood, A. 1997. Trace elements in precious and common opals using neutron activation analysis. *Journal of Radioanalytical and Nuclear Chemistry*, **223**, 9–15.

Papp, G., Sámson, M., Jánosi, M. & Lovas, G. 1998. Mineralogical study of wood opal from Megyaszó (NE Hungary). *Topographia Mineralogica Hungariae*, **3**, 73–83.

Pecover, S.R. 2007. Australian opal resources: outback spectral fire. *Rocks & Minerals*, **82**, 102–115.

Pettke, T. 2008. Analytical protocols for element concentration and isotope ratio measurements in fluid inclusions by LA-(MC)-ICP-MS. *In*: Sylvester, P. (ed.) *Laser Ablation ICP-MS in the Earth Sciences: Current Practices and Outstanding Issues*. Mineralogical Association of Canada, Vancouver, B.C.: Short Course Series, **40**, 189–218.

Peucat, J.-J., Ruffault, P., Fritsch, E., Bouhnik-Le Coz, M., Simonet, C. & Lasnier, B. 2007. Ga/Mg ratio as a new geochemical tool to differentiate magmatic from metamorphic blue sapphires. *Lithos*, **98**, 261–274.

PEWKLIANG, B., PRING, A. & BRUGGER, J. 2008. The formation of precious opal: Clues from the opalization of bone. *The Canadian Mineralogist*, **46**, 139–149.

RAYOT, V. 1994. *Altérations du centre de l'Australie: rôle des solutions salines dans la genèse des silcrètes et des profils blanchis*. Mémoire n°22, Ecole des Mines de Paris.

REN, M. 2004. Partitioning of Sr, Ba, Rb, Y and LREE between alkali feldspar and peraluminous silicic magma. *American Mineralogist*, **89**, 1290–1303.

RONDEAU, B., FRITSCH, E., GUIRAUD, M. & RENAC, C. 2004. Opals from Slovakia ("Hungarian" opals): a re-assessment of the conditions of formation. *European Journal of Mineralogy*, **16**, 789–799.

RONDEAU, B., MAZZERO, F., BEKELE, E., GAUTHIER, J.-P. & FRITSCH, E. 2009. Gem News International: New play-of-color opal from Welo, Ethiopia. *Gems & Gemology*, **45**, 59–60.

RONDEAU, B., FRITSCH, E., GAUTHIER, J.-P., MAZZERO, F., CENKI-TOK, B., BEKELE, E. & GAILLOU, E. 2010*a*. Play-of-color opal from Wegel Tena, Wollo Province, Ethiopia. *Gems & Gemology*, **46**, 90-105.

RONDEAU, B., FRITSCH, E., CENKI-TOK, B. & MAZZERO, F. 2010*b*. New opals from Wollo, Ethiopia: geochemical characterization. *Geochimica et Cosmochimica Acta*, **74**, A880.

ROSSMAN, G.R. 2009. The geochemistry of gems and its relevance to gemology: different traces, different prices. *Elements*, **5**, 159–162.

THOMAS, P.S., BROWN, L.D., RAY, A.S. & PRINCE, K.E. 2006. A SIMS study of the transition elemental distribution between bands in banded Australian sedimentary opal from the Lightning Ridge locality. *Neues Jahrbuch für Mineralogie Abh.*, **182**, 193–199.

ZIELINSKI, R.A. 1982. Uraniferous opal, Virgin Valley, Nevada: conditions of formation and implications for uranium exploration. *Journal of Geochemical Exploration*, **16**, 197–216.

Received 4 November 2010; revised typescript accepted 27 June 2011.